Powder bed fusion with electron beam: The interplay of sintering, porosity, and coordination number in modelling the powder thermal conductivity through a novel

International Journal of Heat and Mass Transfer 234 (2024) 126055

Contents lists available at ScienceDirect

International Journal of Heat and Mass Transfer

journal homepage: www.elsevier.com/locate/ijhmt

Powder bed fusion with electron beam: The interplay of sintering, porosity, and coordination number in modelling the powder thermal conductivity through a novel tortuosity formulation

Giovanni Rizza *, Manuela Galati

Department of Management and Production Engineering (DIGEP), Integrated Additive Manufacturing center (IAM@PoliTo), Politecnico di Torino, Corso Duca degli Abruzzi 24, 10129 Torino, Italy

ARTICLE INFO

Keywords:
Tortuosity
Electron beam melting
Neck
Sintering
Thermal conductivity

ABSTRACT

For the powder bed fusion with electron beam (PBF-EB) additive manufacturing, properties such as the thermal conductivity of the material surrounding the melting area are critical. Thermal conductivity is influenced by the extremely high temperature reached in a short time and distributed in the building area. This fast temperature growth produces sintering phenomena and the creation of a neck between the particles. Because of this sintering, measuring the thermal conductivity at the process conditions is challenging.

This paper proposes an analytical formulation for estimating the effective powder bed thermal conductivity at the PBF-EB conditions, introducing a novel modelling strategy for the tortuosity factor. In a changing net of sintered powder particles, the proposed model for the tortuosity factor considers the neck evolution and the complexity of the heat transfer due to the several heat paths possible through the particle net. To show the effectiveness of the proposed model, the thermal conductivity is evaluated for three 3D structures characterised by an increasing number of powder particles and heat path complexity: a simple cubic, a body centred cubic and a portion of a powder bed. It is shown that thermal conductivity strongly depends on the arrangement of the particles in 3D space, the structure density and the complexity of the heat diffusion path (tortuosity). Also, the numerical results from the proposed model show good agreement when compared with finite element analysis and experimental literature data.

1. Introduction

In powder bed fusion (PBF) additive manufacturing (AM) processes, the characteristics of the final part depend, to a great extent, on the thermal conductivity of the powdered material. The heat dissipation through the surroundings affects the solidification rate of the melted material and the subsequent cooling rate [1], the thermal gradients [2], and, in turn, the residual stresses in the components and the surface quality [3]. In addition, accurate data about the thermal behaviour of metallic powder are crucial for high-fidelity process modelling and forecasts [4]. Typically, the thermal conductivity of the powder is orders of magnitude lower than the corresponding bulk material (e.g. for Ti6Al4V at environment temperature, thermal conductivity is 7.5 $Wm^{-1}K^{-1}$ [5], while the thermal conductivity of the powder in Argon is 0.2 $Wm^{-1}K^{-1}$ [6]). Therefore, the analysis of the thermal conductivity of powders is even more critical for those AM processes in which the low thermal conductivity of the loose powder is detrimental to the material processing. Such a high difference in the thermal behaviour between powder and bulk materials creates strong thermal gradients that could lead to devastating defects in the part, such as thermal cracks [7]. To overcome this issues, in some cases, as for the powder bed fusion with electron beam (PBF-EB) process, the thermal conductivity of the powder bed is enhanced by slightly sintering each layer with a preheating conducted at a high heating rate (approximately 15 °C/s [8]). The preheating phase and the vacuum environment in the PBF-EB maintain a hot environment and allow crack-prone material processing. However, these thermal conditions promote a super-fast sintering process occurring at the solid state and allowing the formation of a small bridge of material among adjacent particles of the powder bed. These solid connections, called necks, are then responsible for the heat conduction among the particles. As an example, Liu et al. [9] showed that the thermal conductivity of the particles above a certain temperature,

* Corresponding author.
E-mail address: giovanni.rizza@polito.it (G. Rizza).

https://doi.org/10.1016/j.ijheatmasstransfer.2024.126055
Received 21 May 2024; Received in revised form 17 July 2024; Accepted 8 August 2024
Available online 19 August 2024

presumably the sintering starting temperature, increases rapidly according to the material nature. This is the case of the Ti6Al4V for temperatures above 600 °C [9]. In this condition, the powder bed can be pictured as a net of interconnected particles with voids.

The issue of thermal conductivity in two-phase powder beds is widely discussed in the literature. Examples of such studies can be found in Ref. [10–12] and in a comprehensive literature review provided by Tsotsas and Martin [13]. These analyses typically focus on the presence of gas and strongly sintered materials, a condition often achieved by applying pressure [14]. The powder bed is usually packed using a mechanical external load as a vibration [15]. Also, the particles may be shaped in a wide range of geometries as hexagonal or triangular prism. These factors significantly influence thermal conductivity [15] and are far from the characteristic of AM processes based on powder bed fusion. This is particularly true for PBF-EB, where the process uses spherical particles, occurs in a high vacuum, the particles are gently distributed to form the powder bed, and the sintering of the particles is weak. In this context, attempts to analyse the thermal conductivity of AM powder bed were performed using experimental, mixed experimental and numerical or numerical/analytical techniques.

On the experimental methods, Presley and Christensen [16] provided a detailed review of the measuring methods and techniques for particle material. Most of them, such as the transient hot wire and laser flash, can be easily adapted to the AM processes in which the working conditions are at environment temperature and under inert gas, such as in the case of powder bed fusion processes with a laser beam [4,6]. At higher working temperatures, when the sintering process is activated, the application of standard methodologies becomes more challenging. Gong et al. [17] used a thermal analyser to measure the thermal conductivity of Ti6Al4V powder sintered by preheating with a PBF-EB process. The measured thermal conductivity was lower than the corresponding bulk material and depended on the sintering temperature. The same results were found by Neira Arce [18], who evaluated the thermal conductivity of Ti6Al4V powder produced with the plasma rotating electrode process (PREP) and gas atomisation (GA) using a laser flash technique. The measurements were performed by varying the temperature up to 1600 °C and normal pressure in an argon atmosphere. Also, in this case, the thermal conductivity remained unvaried up to 600 °C. Above 600 °C, the thermal conductivity increased rapidly. The PREP powder showed the lowest thermal conductivity due to the smaller mean diameter. The difference between the two powders increased with the temperature, achieving a difference of approximately 30% at 1600 °C. Smith et al. [19] also used the laser flash technique to measure the thermal conductivity of sintered powder samples for different PBF-EB process parameters. The powder material sintered with higher energy (e.g. a higher number of beam passages) showed a higher thermal conductivity, presumably due to the larger necks. Galati et al. [20] used the laser flash technique to measure the thermal conductivity of Ti6Al4V samples that entrapped different thicknesses of partially sintered powder maintained in vacuum conditions. The thermal conductivity was measured at different temperatures (up to 800 °C). The authors showed that the thermal conductivity is independent of the thickness of the powder contained in the sample. Owing to the complexity of emulating the working conditions during a PBF-EB, all the studies based on pure experimental approaches were performed using pre-sintered powder. Thus, they were not able to capture the time-dependent dynamical variations of the thermal conductivity that takes place in a fast heating process such as PBF-EB.

Leung et al. [21] applied a combined experimental-numerical approach to study samples produced by PBF-EB and entrapping sintered Ti6Al4V powder. After the production, the samples were analysed using an X-ray computed tomography scan (CT-Scan), and the 3D reconstruction was then used as input for the numerical models. The thermal conductivity was calculated from a numerical model based on the mean properties of the powder bed [22] and a numerical model based on the thermal tortuosity generated by the presence of the sintering necks among the particles [23].

Pure numerical analyses were applied by Chua et al. [24] using a finite element (FE) model on two powder particles, without necking, to calculate the thermal conductivity under a linear evolution of the temperature. Considering the actual geometry of the particles when the sintering occurs, Gusarov et al. [25] proposed a numerical model in which the thermal conductivity is scaled according to the relative density of the powder bed, the coordination number, and the dimension of the neck between the powder particles. These geometrical quantities were evaluated for simple and ordered structures and equal particles, while the application became difficult for a random particle size distribution. Grose et al. [26] used a simple phase field (PF) model to calculate the necking. The geometrical information was transferred to a FE model to perform steady-state heat transfer simulations. In this case, the particles were polymeric. The transfer of the information from the sintering simulation to the thermal conductivity calculation was computationally expensive and required several adjustments. Moreover, the material parameters and the temperature evolution to set up the PF simulation were not reported.

In view of the literature, the main challenges still remaining are the possibility of gathering real-time information on the evolution of the powder bed over time and during real process conditions, and transferring this information in an affordable and simple method to calculate thermal conductivity. For the first issue, PF simulations have been demonstrated to be able to emulate the sintering and neck growth if the temperature and powder bed topology are implemented in a realistic way [27]. For the second issue, it is essential to develop a thermal conductivity formulation that accurately captures the effect of the material geometry variation on the heat conduction rate through the net of particles created by the necks. An analytical formulation may address this issue, whereas using FE models would demand significant efforts to apply properly the heat load [19] and to model and update the complex net geometries that evolve with the neck growth [26].

The basic principle is that thermal conductivity measures the ease of heat flow through the material. For bulk material, this property is strictly related to the intrinsic characteristics due to the elastic vibrations of the lattice and the free electrons that move through the lattice carrying energy. The number of vibrations and energy depend on the temperature. For a sintered powder, the heat should flow through the solid net, which varies with the temperature. Because of this continuous evolution, similar to the description of the complexity of the fluid flow in hydraulic applications, an analytical method may support the analysis [28]. An index that can measure this complexity is tortuosity. An example of the use of tortuosity for fluid flow path within a porous material is given in the work by Ahmadi et al. [29]. Montes et al. [30] applied this concept to a thermal problem and defined thermal tortuosity as the ratio between the length of a porous material in the direction of the heat flux (L_t) and the length of the shortest path within the solid material that the flow should cover from the inlet to outlet (L_d). A clarification of this concept is illustrated in Fig. 1. However, this definition has a limitation: many paths are practicable, and each path within the particles is much longer than L_d. The complexity increases when 3D structures are considered.

Leung et al. [21] used an open-source application, TauFactor [23], which calculates the tortuosity by measuring the heat flow through a 2D image of the porous media. Such a method may consider the flux through the connection between particles, but the resulting tortuosity value is affected by the dimension of the inlet area and the presence of an empty area in the 2D image [21].

In this work, the thermal conductivity is evaluated by proposing an analytical method based on a novel definition of the tortuosity index for particles interconnected by necks. In this way, the calculation of the thermal conductivity of the powder bed can continuously consider the sintering evolution during the process. The application of the proposed methodology is shown for the evaluation of the thermal conductivity of three case studies with increasing complexity: a simple cubic structure

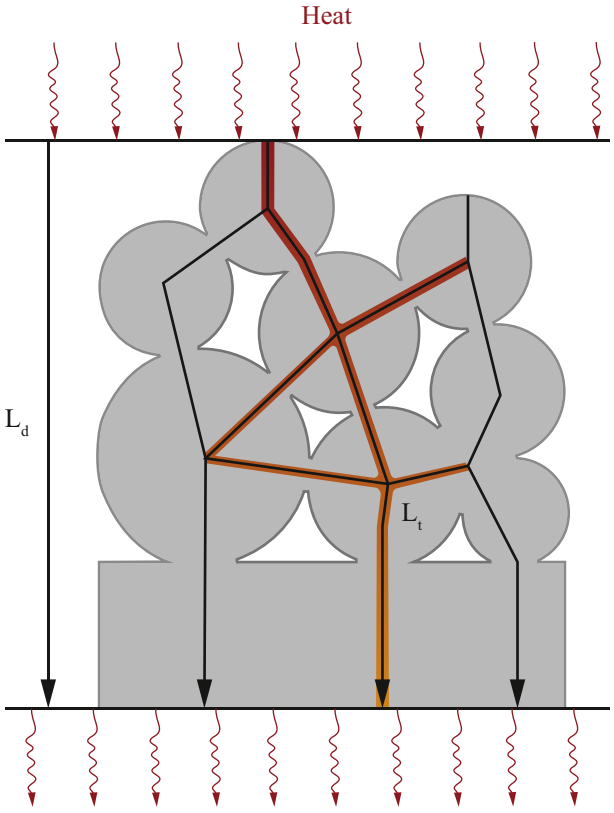

Fig. 1. Possible heat path within a structure representative of a powder bed.

(SC), a body centred cubic structure (BCC), and a portion of a randomly distributed powder bed (PB). For PB, particles with different diameters are also considered. The results are compared against numerical data obtained from FE calculations and literature data. The material considered is Ti6Al4V.

2. The tortuosity factor and the thermal conductivity model

As mentioned above, initially, tortuosity was introduced to describe the flow of a fluid through the voids of a porous media [31]. Only lately, it has also been used to evaluate the thermal or electrical conductivity in a porous material [21,30], as it measures the complexity of the path that the heat flow must follow to transport the energy from the hot to the cold side of the material. The higher the tortuosity, the lower the thermal conductivity. This concept is expressed by Eq. (1) according to Ref. [32], in which the thermal conductivity of a porous material (λ_{pow}) is connected to the thermal conductivity of the bulk material (λ_0), considering the relative density of the structure (n) and the tortuosity of the system (τ^2).

$$\lambda_{pow} = \frac{n}{\tau^2}\lambda_0 \tag{1}$$

Eq. (1) is valid under the following limiting cases (Eq. (2)) [29,30]:

$$\begin{cases} \tau > 0 \\ \tau^2 \geq 1 \\ \lim_{n\to 1} \tau^2 = 1 \\ \lim_{n\to 0} \tau^2 = \infty \end{cases} \tag{2}$$

With this definition and considering the description of τ^2 in the literature (Fig. 1), when the path in the porous material is complex, τ^2 should tend to be infinite and λ_{pow} to zero. When the porosity in the porous material is small, the flux should be facilitated and, at the limit, L_t tends to L_d and, therefore, τ^2 should tend to 1. When τ^2 tends to the unity, λ_{pow} tends to λ_0 [29,30].

However, this definition becomes limiting for the 3D characteristics of the powder bed in PBF-EB, which also evolves with the formation of the necks. In this case, defining a unique path is not feasible because the heat transmission is inhomogeneous and depends on factors such as the particle size, the evolution of the neck size, and the number of contact points of the particles.

To address these aspects, a defined 3D control volume that encompasses the entire powder bed for PBF-EB or a selected portion of it, named representative elementary volume (REV), is assumed. This REV should be characterised by symmetry in the xy plane, with the z-aligned with the build direction in the PBF-EB process. The control volume (or REV) represents the calculation domain and should also respect the following hypotheses:

- The total volume occupied by the porous material consists of two phases: a persistent solid phase consisting of the particles and an empty space consisting of voids between the solid particles.
- The particles are homogeneously distributed over the domain.
- All the particles should be connected to create a flux of heat. This means that it is possible to identify at least one line of flux between any two points on the domain, and the line lies entirely in the solid domain.

Considering all the premises above, a new formulation of τ^2 is expressed as a function of three contributions (Eq. (3)): the portion of the active surface in the domain that can transmit the heat, the geometry of the constrained section formed by the neck, and the relative density of the structure, including the contact points of each particle.

$$\tau^2 = f\ (\text{active surface},\ \text{constrained section},\ \text{n(contact particle points)}) \tag{3}$$

The first and third contributions could represent the structure, while the constrained section could describe local information on heat transfer. The active surface enabling heat transfer is the parameter that accounts for the inlet and outlet sections of the domain that can conduct heat. Therefore, it can be evaluated as the ratio between the fraction of the lateral area occupied by solid material (S_{SS}) and the total lateral surface area of the domain (S_0).

The third contribution considers n, the relative density of the domain (or REV), which is complementary to the porosity. It is calculated as the ratio of the total volume of solid material in the domain (U_{0s}) and the total volume of the domain (U_0).

Fig. 2 graphically shows the geometrical quantities measured in a portion of the domain composed of spherical particles with the same diameter, arranged according to a simple cubic structure. In this case, U_0 and S_0 are the volume and the surface of the cube, representing the boundary of the domain (or REV). At the beginning, U_{0S} (cf. Fig. 2(a)) is the sum of the volume of the powder particles. When the sintering occurs

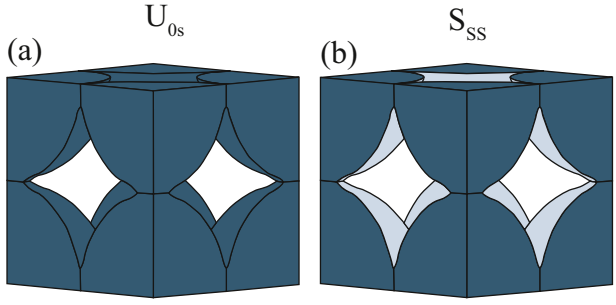

Fig. 2. Representation of the geometrical quantities for the calculation of γ and n. (a) in dark blue, the volume of the solid material within the domain (U_{0S}). (b) in dark blue, the surface that is created by the intersection of the particles and the predefined domain (S_{SS}).

and a neck is formed and growing, U_{0S} varies according to the neck dimension and can be evaluated as the sum of the volume of the powder particles and the volume of the neck. This methodology also applies to S_{SS} (cf. Fig. 2(b)). At the beginning of the process, these quantities are given as the sum of the surfaces and volumes of the spherical powder particles. In the following stages, the neck geometry is included in the calculations.

For particles connected by necks, the hypothesis of Eq. (2) suggests that τ^2 should approach infinity when the particles are not sintered, and the ratio of solid material to void is minimal ($n \to 0$). Conversely, τ^2 should approach unity for a fully dense component ($n \to 1$), indicating that all voids are closed or the heat flows directly through the shortest path, corresponding to L_d in Fig. 1. Consequently, the contribution of n must be included so that τ^2 is inversely proportional to n.

However, as the number of contact points between particles increases, the heat flow path becomes more complex. Similar to an electrical circuit, in a particle with multiple contact points, the heat flux divides into different branches (e.g., the highlighted paths in Fig. 1). Practically, this complexity reduces the effect of n in reducing τ^2. In a domain composed of only two particles with a single contact point, the heat flows directly through the contact point, depending purely on n and the constrained section.

An effective way to account for this complexity is to use a power law where the exponent of n is adjusted by a descriptor, which accounts for the number of contact points among the particles, denoted as φ. This parameter could be assumed to be related to the particle's coordination number. Since φ influences the total heat flow branches in the domain, in this work, it is assumed to be equal to worst condition for the heat and therefore equal as the particle with the highest coordination number (highest number of particles bonded to a single particle, e.g., in Fig. 1, φ is equal to 5).

The contribution of the constricted section to the heat flow can be represented by the neck formed between two particles. In a domain of various particles, the neck size depends on the two particles forming it. Locally, analogous to fluid localised head losses, the shape of the constricted section for heat flow through two contacting powder particles is defined geometrically using a factor named γ, as reported in Eq. (4):

$$\gamma = \frac{D - 2x}{D} \tag{4}$$

As sintering advances, the neck size (x) increases, facilitating the heat flow through the constrained section created by the neck and causing γ to decrease. When sintering occurs between particles of the same diameter, the neck dimension is uniform for each pair of particles [27], resulting in a consistent tortuosity value across the domain. However, in the case of sintering among particles with different diameters, identifying the primary obstacle to heat flux, which leads to the lowest thermal conductivity, is more complex. Both the neck size and the ratio between the neck size and particle size must be considered simultaneously.

Using γ as defined simplifies this process. The most constrained section can be uniquely identified by considering the pair of particles with the highest ratio between the neck size and the diameter of the particles. Locally, γ is calculated using the particle with the largest diameter among the two forming the neck, as this represents the sharpest variation for the heat flow and, therefore, the most challenging condition for heat transfer. Fig. 3(a) and (b) represent graphically, with a 3D and 2D view, respectively, the local geometrical quantities related to a couple of powder particles forming the neck. x is the neck radius, measured as the distance between the absolute minimum of the lateral surface of the neck and the straight line passing through the centres of the powder particles. D is the diameter of the largest powder particle in the couple.

Based on the above discussion, the new formulation of τ^2 is presented in Eq. (5).

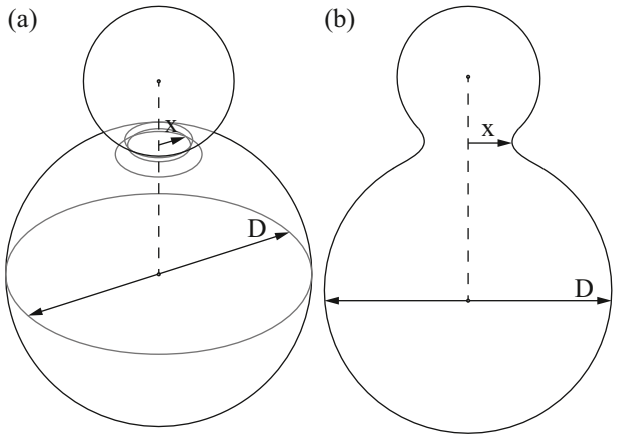

Fig. 3. (a) 3D and (b) 2D view of a couple of partially sintered powder particles. x is the neck radius. D represents the diameter of the largest powder particle of the couple.

$$\tau^2 = \frac{S_{ss}}{S_0}\gamma n^{(1-\varphi)} \tag{5}$$

All the geometrical quantities describing the complexity of the path are a function of the sintering evolution. Therefore, the remaining point becomes to obtain information about the sintering. As mentioned above, this data could come from experimental or numerical sources, e.g., a phase field model [27].

Fig. 4 represents a possible workflow to move from the geometry of the sintering powder particles to the evaluation of thermal conductivity using a phase field simulation. The inputs are the initial topology of the domain, the material properties, and the thermal history. The initial topology of the structure may be obtained from CT scans. From the topology, the coordination number φ can be evaluated. At each time step or predefined major time step and until the end of the process (t_{end}), the phase field simulation is used to calculate the neck growth. For each pair of particles in the simulation domain (i_{tot} is the total number), the neck radius for each pair of particles is extracted. Then γ is calculated (Eq. (4)) and the geometrical quantities (S_{ss}, U_{0S}) are evaluated. With this information, $\frac{S_{ss}}{S_0}$ and n are evaluated. These numerical data allow the calculation of τ^2 (Eq. (5)) and λ_{pow} (Eq. (1)).

3. Case studies

The framework summarised in Fig. 4 was applied to show the calculation of the thermal conductivity of three structures that are characterised by an increasing number of powder particles and heat path complexity. The structures considered were the simple cubic (SC), the body centred cubic (BCC) and a portion of a powder bed (PB) in typical PBF-EB process conditions. The SC and the BCC are considered because they are commonly adopted in literature to simplify the powder bed topology [25,33,34]. The structure representing a portion of a powder bed consisted of randomly organised powder particles with different diameters, as in a real powder bed. In all the structures, the diameter of the powder particles ranged from 45 μm to 150 μm, representing the standard size distribution of powder processed in a PBF-EB process [3].

Information about the neck geometry evolution was calculated using a phase field simulation [27], in which the sintering occurs only by atomic diffusion mechanisms. The sintering was simulated under the temperature ramp-up according to Eq. (6). The ramp-up was assumed to follow the preheating of a PBF-EB process and increase in steps [27].

$$T(t) = T_{bp} + \mathrm{int}\left(\frac{t - t_{bp}}{t_p - t_{bp}} s\right) \frac{T_p - T_{bp}}{s} \tag{6}$$

where:

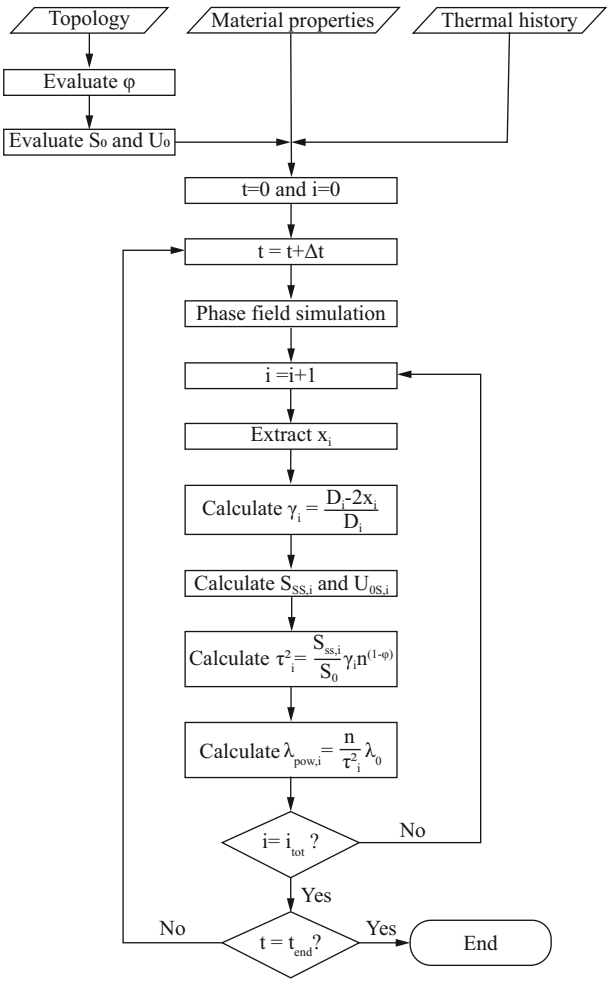

Fig. 4. Workflow for the evaluation of thermal conductivity according to the model presented. t_{end} is the total simulation time. i_{tot} is the total number of pairs of particles in the simulation domain.

- T_{bp} is the initial powder temperature before the preheating and was assumed to be 845 K.
- t_{bp} is the initial time and was assumed to be zero.
- t_p is the entire duration of the preheating and was assumed to be 9.5 s [27]
- T_p is the temperature at the end of the preheating step and was assumed to be 1273 K [35].
- s is the number of steps to increase the temperature from T_{bp} to T_p and was set equal to 25.

The time steps with the corresponding temperature at the end of the steps are reported in Table 1. Further details about the phase field modelling can be found in Ref. [27].

Table 1
Values of λ_0 for the bulk Ti6Al4V adopted for the evaluation of λ_{pow} in all the case studies.

time [s]	Temperature [K]	λ_0 [$Wm^{-1}K^{-1}$]
0.5	879	11.52
1.5	913	11.97
2.5	964	12.64
3.5	1016	13.33
4.5	1050	13.78
5.5	1101	14.45
6.5	1153	15.14
7.5	1187	15.59
8.5	1239	16.27
9.5	1273	16.72

Considering the sintering as the diffusion of atoms from different parts of the powder particles to the neck region, no distinct interface is assumed between the particles. Thus, the phase field model includes the solid material and the empty space among the powder particles, which has no contribution to thermal conductivity due to the vacuum environment characteristic of the PBF-EB.

The material selected for the case studies was Ti6Al4V, for which the value of λ_0 [36] was assumed to be temperature-dependent, as reported in Table 1.

3.1. Thermal conductivity evaluation of a simple cubic (SC) structure

This case study assumes a sintering process of particles arranged according to a simple cubic (SC) structure. Geometrically, the particles were supposed to be organised as follows. Each particle has the same diameter equal to 80 μm. The centre of a powder particle was positioned at each node of a regular cubic grid. Therefore, the lateral size of the elementary cell corresponds to the particle diameter. At the beginning of the sintering, the powder particles are in contact only at a single point; no neck is present. The domain used for the calculation corresponded to a single cell of the grid and, therefore, consisted of eight parts of eight powder particles. Fig. 5 shows the particles at the initial stage of the sintering (no neck).

The sintering process was simulated under the temperature profile presented in Eq. (6), and the geometrical information about the neck growth was extracted every second from the initial neck growth at 0.5 s (Table 2, third column).

In this case, the domain is a simple cube; therefore, the total volume U_0 and the total surface S_0 are constant during the sintering and equal to 512,000 μm^3 and 38,400 μm^2, respectively. The value of φ (Eq. (5)) is equal to 3 because each particle is in contact with three other particles. Table 2 reports the values of U_{0s} and S_{SS} at each time of acquisition. With the values of volume U_{0s} reported in Table 2, n is equal to 0.52.

Besides the geometrical data, Table 2 also reports the calculated γ (Eq. (4)), τ^2 (Eq. (5)), and the corresponding thermal conductivity λ_{pow} (Eq. (1)). Fig. 6 compares the evolution of the neck radius with the corresponding tortuosity and thermal conductivity.

Considering the values reported in Table 2 and Fig. 6, it is possible to notice that the neck radius (x) among the particles grows at each step with the temperature. Initially, the neck grows rapidly, while the growth ratio drops after 3.5 s and proceeds with a constant growth ratio of around 0.3 μm/s. It follows that γ also decreases constantly, representing an easier heat conduction. As a result, τ^2 decreases constantly from 2.62 to 2.33, with a resulting thermal conductivity increase from 2.30

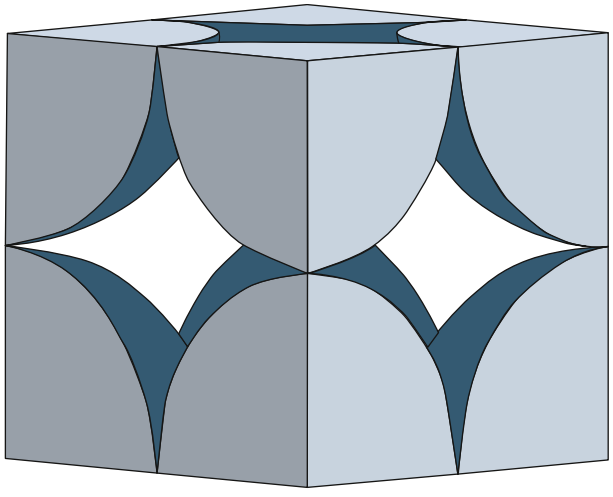

Fig. 5. SC structure at the initial stage of the sintering (no neck).

Table 2
eometrical data relative to the SC domain (U_{0s} and S_{SS}). Values of γ, τ^2 and λ_{pow} for the SC structure.

time [s]	Temperature [K]	x [μm]	U_{0s} [μm^3]	S_{SS} [μm^2]	γ	τ^2	λ_{pow} [Wm^{-1}K^{-1}]
0.5	879	3.84	267,750	30,530	0.90	2.62	2.30
1.5	913	5.40	267,153	31,150	0.86	2.56	2.45
2.5	964	6.31	266,764	31,570	0.84	2.53	2.62
3.5	1016	6.80	267,477	30,984	0.83	2.44	2.86
4.5	1050	7.28	268,141	32,174	0.82	2.50	2.89
5.5	1101	7.48	266,871	31,706	0.81	2.45	3.09
6.5	1153	7.95	268,765	31,619	0.80	2.40	3.31
7.5	1187	8.19	268,237	31,496	0.80	2.37	3.45
8.5	1239	8.42	268,994	31,334	0.79	2.34	3.65
9.5	1273	8.62	267,492	31,240	0.78	2.32	3.79

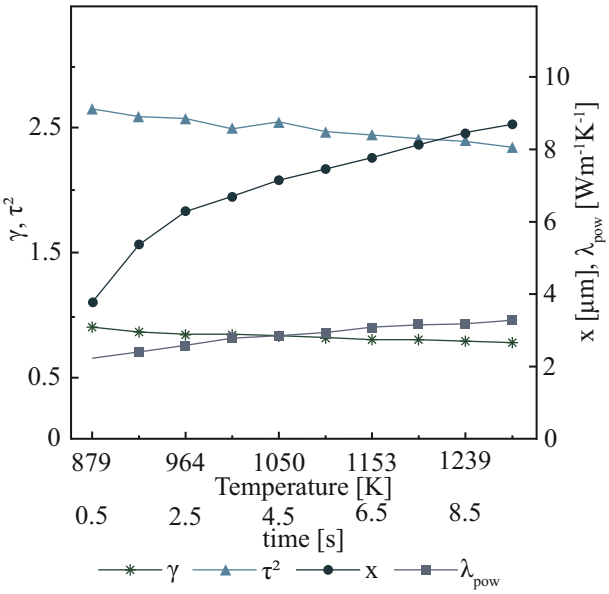

Fig. 6. Geometrical factor (γ), tortuosity (τ^2), neck radius (x), and thermal conductivity (λ_{pow}) during the sintering of a SC structure.

Wm^{-1}K^{-1} to 3.75 Wm^{-1}K^{-1}.

3.2. Thermal conductivity evaluation of a body centred cubic (BCC) structure

This case study considers the sintering of powder particles arranged according to a body centred cubic (BCC) structure, with a dimension of the elementary cell equal to 80 μm. Therefore, as in the previous case, the powder particles positioned with centres on the nodes of a regular cubic grid have a diameter equal to 80 μm. In addition to the previous case, the body in the centre is a powder particle designed to fill the central space of the regular grid of powder particles with a diameter of 80 μm. The corresponding diameter of the central particle is 58.6 μm.

At the beginning of the sintering, the powder particles are in contact with the others at a single point; no neck is present. The domain (Fig. 7) adopted for the calculation corresponded to a single cell of the grid and, therefore, consisted of eight portions of eight powder particles with a diameter of 80 μm and the smaller powder particle in the centre with a diameter of 58.6 μm.

As in the previous case, the sintering process was simulated under the temperature profile described in Eq. (6), and the geometrical information about the neck was extracted every second for each couple of particles: couple 1 and couple 2. Couple 1 represents the couple made of particles with the same diameter and equal to 80 μm, and couple 2 consists of a powder particle with a diameter of 80 μm and a powder particle with a diameter of 58.6 μm.

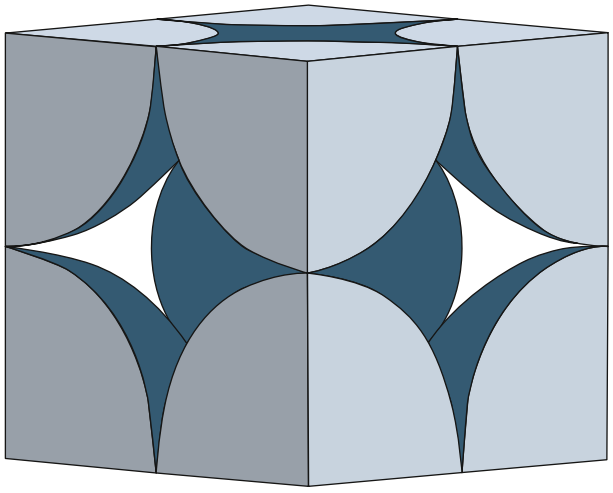

Fig. 7. BCC structure at the initial stage of the sintering (no neck).

Table 3 reports the neck radius extracted from the sintering simulation for couples 1 and 2. Since couple 2 involves a smaller particle, the neck formed in couple 1 is always larger than the neck between couple 2, in agreement with Ref. [37].

Similar to the SC case, also in this case, the domain is a simple cube with the total volume (U_0) and the total surface (S_0) equal to 512,000 μm^3 and 38,400 μm^2, respectively.

The structure presents different neck values as a function of the couple of particles considered for the calculation. Also, for couple 1, each particle is in contact with another particle at 4 points. The central particle belonging to couple 2 has 8 contact points. This value is therefore set for both couples as φ for Eq. (5). Owing to the different dimensions of the neck formed among the particles, the tortuosity value has been calculated considering the highest value of neck (couple 1) and smallest (couple 2).

In this case, necks are formed also between particles with different diameters. However, since γ was defined as the difficulty for the heat to

Table 3
Geometrical information on the neck evolution for couple 1 and couple 2.

time [s]	Temperature [K]	Couple 1 (80 – 80) x [μm]	couple 2 (80 – 58.6) x [μm]
0.5	879	3.84	4.26
1.5	913	5.40	5.31
2.5	964	6.31	5.96
3.5	1016	6.80	6.38
4.5	1050	7.28	6.70
5.5	1101	7.48	7.02
6.5	1153	7.95	7.25
7.5	1187	8.19	7.64
8.5	1239	8.42	7.90
9.5	1273	8.62	8.09

go through the neck, the most critical condition is assumed considering the largest particle in each couple. Therefore, D in Eq. (4) is assumed to be equal to 80 μm.

Tables 4 and 5 show the geometrical values, γ, the corresponding τ^2 and the thermal conductivity (λ_{pow}) at each acquisition time for couples 1 and 2, respectively. For this structure, n was equal to 0.72. Fig. 8 compares the evolution of neck radii with the corresponding γ, tortuosity and thermal conductivity of the BCC structure during sintering.

Regardless of the considered couple, the neck radius grows with the temperature. As mentioned above, the neck for couple 2 is always smaller, while the result at the first step may be due to numerical errors. Since the diameter considered for the particles in γ was the same, the differences between the couples of particles can be observed only when the neck size becomes significantly different (around 2.5 s). Similarly to the neck, γ decreases with the same ratio among the couple of particles. As expected, γ is higher when considering couple 2, for which a combined effect of a smaller neck and a more constrained section occurs. It follows that τ^2 decreases for both couples. The decrease of τ^2 produces an increase of the thermal conductivity, which is always lower for couple 2. However, because the couples of particles considered in the case study have similar dimensions, and produced comparable necks and neck growths, also φ is considered fixed and equal to the coordination number of the central particle, the difference among the thermal conductivity values results almost negligible (below 1 %). Over the different time steps, the thermal conductivity goes from 1.29 $Wm^{-1}K^{-1}$ to 2.25 $Wm^{-1}K^{-1}$, around one order of magnitude lower than the corresponding value for the bulk material at the same temperature (Table 1). The obtained values agree with the results reported in [34] for the same material, same particle arrangement and similar packed density, considering, however, particles with the same diameter and neglecting neck growth.

3.2.1. Comparison with finite element method

A finite element simulation has been implemented to verify the capability of the analytical model proposed in this work. Finite element models are widely used for addressing thermal problems for isotropic material [38], for which the resulting overall thermal conductivity is also isotropic. With FE, the temperature gradient across the structure and the relative heat flux need to be determined using the geometrical model. Then the thermal conductivity can be calculated using the Fourier's law (Eq. (7)):

$$q = \frac{\lambda A \Delta T}{L} \tag{7}$$

where q is the heat power, measured in W, A is the area crossed by the heat flux, ΔT is the thermal gradient between the hot (surface at higher temperature) and cold (surface at lower temperature) surfaces, and L is the length of the sample. However, for complicated and anisotropic structures, geometry is a critical factor that determines the deviation from the principal direction of the thermal gradient. While the methodology proposed in this paper gives an indication of the contact thermal conductivity as a structural property rather than an intrinsic thermal property of the material, the implementation of a complex structure by an FE model requires hypotheses on the selection of the hot and cold surfaces and how the heat is measured.

Considering the structure as oriented in Fig. 7, a thin squared plate has been added to apply the temperature boundary conditions at the top and the bottom surfaces, according to Li et al. [39]. The dimensions of each plate were 80 μm × 80 μm × 5 μm. Temperature boundary conditions were applied to the two plates, as shown in Fig. 9. The top plate was defined as the hot surface, while the bottom was set as the cold surface. The temperature of the hot surface was set equal to the temperature reached at the end of the considered time step in the PF simulation (Table 1), while the temperature of the cold surface was set to obtain ΔT equal to 1 K. The mesh for each structure adopted tetrahedral elements with a maximum size equal to 5 μm. The thermal conductivity of the bulk material has been set according to the corresponding simulated hot temperature, as given in Table 1. The FE analysis was therefore set up to simulate a three-dimensional steady-state thermal analysis and was performed using SolidWorks 2021. Since the use of FE requires a

Table 4
Geometrical data relative to the domain (U_{0s} and S_{SS}), γ, τ^2 and λ_{pow} when considering couple 1 (80 μm - 80 μm). γ is calculated considering the particle with a diameter equal to 80 μm.

time [s]	Temperature [K]	U_{0s} [μm^3]	S_{SS} [μm^2]	γ	τ^2	λ_{pow} [$Wm^{-1}K^{-1}$]
0.5	879	372,974	30,530	0.90	6.53	1.29
1.5	913	372,292	31,150	0.86	6.40	1.36
2.5	964	371,616	31,570	0.84	6.35	1.45
3.5	1016	372,280	30,984	0.83	5.97	1.63
4.5	1050	372,346	32,174	0.82	6.19	1.63
5.5	1101	371,232	31,706	0.81	6.05	1.74
6.5	1153	373,891	31,619	0.80	5.76	1.93
7.5	1187	372,182	31,496	0.80	5.66	2.02
8.5	1239	371,833	31,334	0.79	5.48	2.19
9.5	1273	370,005	31,240	0.78	5.46	2.25

Table 5
Geometrical data relative to the domain (U_{0s} and S_{SS}) γ, τ^2 and λ_{pow} when considering couple 2 (80 μm −58.6 μm). γ is calculated considering the particle with a diameter equal to 80 μm.

time [s]	Temperature [K]	U_{0s} [μm^3]	S_{SS} [μm^2]	γ	τ^2	λ_{pow} [$Wm^{-1}K^{-1}$]
0.5	879	372,974	30,530	0.89	6.46	1.30
1.5	913	372,292	31,150	0.87	6.47	1.35
2.5	964	371,616	31,570	0.85	6.42	1.43
3.5	1016	372,280	30,984	0.84	6.04	1.61
4.5	1050	372,346	32,174	0.83	6.27	1.61
5.5	1101	371,233	31,706	0.82	6.12	1.72
6.5	1153	373,890	31,619	0.82	5.91	1.88
7.5	1187	372,182	31,496	0.81	5.73	2.00
8.5	1239	371,833	31,334	0.80	5.55	2.16
9.5	1273	370,004	31,240	0.80	5.60	2.20

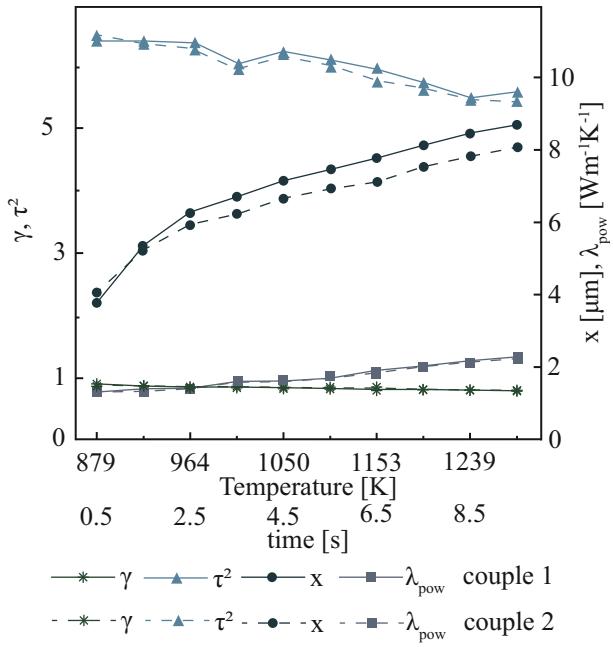

Fig. 8. Geometrical factor (γ), tortuosity (τ^2), neck radius (x), and thermal conductivity (λ_{pow}) during the sintering of the sintering of a BCC structure calculated considered couple 1 and couple 2.

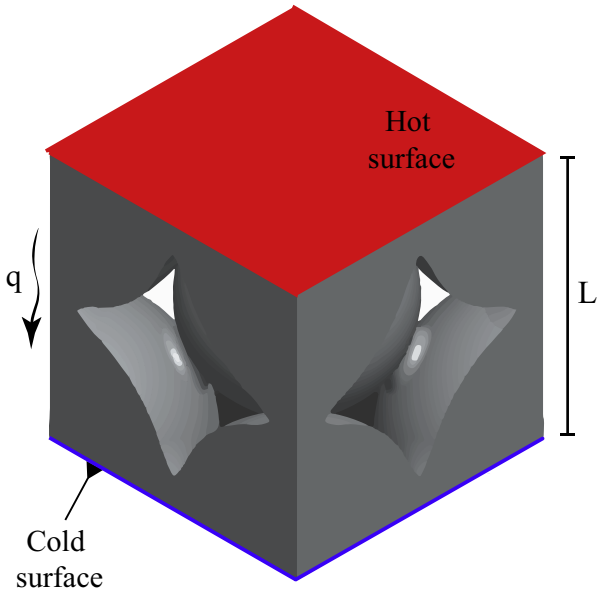

Fig. 9. Schematic diagram of boundary condition and modelling using finite element method.

complex remodelling of the structure at each increment of neck growth, the verification was limited to three steps of the sintering (2.5 s, 5.5 s and 9.5 s) corresponding to a temperature of 964 K, 1101 K and 1273 K, respectively.

As an example, Fig. 10 shows the temperature distribution in the structure at 9.5 s (hot surface at 1273 K), in which the top and bottom plates have been removed.

Table 6 compares the thermal conductivity obtained by the FE analysis with the value from the proposed numerical model, extracted as an average for each time between the values provided in Tables 4 and 5. As observed, the analytical model captures the effect of temperature on thermal conductivity, particularly considering the presence of smaller particles that act as bottlenecks for heat transfer. In fact, the analytical model shows an increase in thermal conductivity by the temperature and neck size comparable with the FE results. However, as it can be noted, the values from the FE analysis are higher than the corresponding analytical values. This discrepancy may result from several factors inherent to the FE analysis, such as the CAD modelling accuracy, the discretisation or the impossibility of updating the neck evolution directly. Besides that, it is important to note that the parameter φ becomes particularly significant for couple 1, where the particles have a lower coordination number than the assumed φ (4 vs 8). This

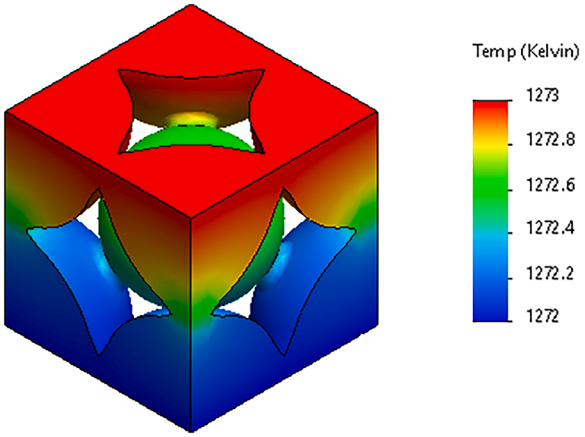

Fig. 10. Temperature distribution for the structure sintered at 1273 K.

assumption substantially reduces the thermal conductivity values, which would range between approximately 4.56 $Wm^{-1}K^{-1}$ and 7.59 $Wm^{-1}K^{-1}$ if φ was considered equal to 4. Therefore, the impact of φ is critical when the structure comprises particles with varying coordination numbers. Consequently, the FE analysis yields values that lie between the extreme values dictated by the coordination numbers characterising the particle of the structure.

3.3. Thermal conductivity of a powder bed (PB)

This case study analyses a representative portion of a powder bed (PB) consisting of randomly packed spherical particles. Fig. 11 shows the domain of calculation, composed of 13 powder particles or a portion of them, with different diameters randomly distributed in a cubic space. The diameter of these powder particles ranged between 45 μm and 150 μm, which is a typical particle size processed in a PBF-EB process [3]. For easy reference, each particle was indexed by a number (Fig. 11 and Table 7). Table 7 reports the diameter of each particle of the domain.

According to the modelling hypothesis, each powder particle of the structure is in contact at least with another particle. For example, particle 9 (Fig. 11 and Table 8) has the largest number of contact points; specifically, it is in contact with particles 1, 5, 6, 7, 8, 10, 12 and 13. Two adjacent particles form a couple identified by an ID composed of the corresponding diameters of the particles composing the couple, as reported in Table 8. The dimension of the domain (REV) considered is 150 μm, according to the height of the powder layer before the melting [40]. The sintering process was simulated under the temperature profile described in Eq. (6). The results of PF simulations are reported in Table 8. Because of the complexity of the structure, the neck dimensions for each couple of powder particles were extracted only at 0.5 s, 3.5 s, 6.5 s and 9.5 s. As can be observed, the neck increases rapidly from 0.5 s to 3.5 s, while the neck growth rate slows down as the simulation continues. These results are in agreement with Ref. [37]. The dimension of the neck radius is connected to the particle diameter ratio, assumed as the ratio of the diameter of the smaller particle divided by the diameter of the larger particle. Couples with a bigger diameter ratio have a larger initial neck and neck growth rate. As an example, considering the couple 1–2, which has a diameter ratio of 1, and the couple 9–12, that have a diameter ratio of 1.5 at 3.5 s of the simulation, the neck radius is double for the couple 9–12 with respect to the couple 1–2.

For the PB structure, the total volume and the total surface of the REV were U_0=3,375,000 μm^3 and S_0=135,000 μm^2, respectively. In this case, φ=8 (Eq. (5)) is the largest number of contacts inside the domain. S_{SS} is equal to 70,714 μm^2. U_{0s} increases from 2,236,055 μm^3 at 0.5 s to 2,239,506 μm^3 at 9.5 s. n was assumed constant and equal to 0.66. τ^2 was calculated considering the diameter of the largest particles composing the couple. As an example, in the case of 150–60, D was set equal to 150 μm. Tortuosity and thermal conductivity values depend on the couple of powder particles. The calculation considered all the couples and the related geometrical data (D and x). The results are collected in Table 9 and shown graphically as variation bands in Fig. 12.

At the beginning of the sintering, the size of the necks is small and comparable for each couple of particles. This produced, in most cases and, in particular for couples of particles with a comparable diameter, comparable values of γ and τ^2 among the couples (e.g. 80–80, 80–75, 80–74) and the highest thermal conductivity values. When the differences between the diameters of the particles is larger, the γ and τ^2 are also larger; therefore, the conductivity is lower. (e.g. 55–150)

When the neck grows, the combined effect between the particles composing the couple and the corresponding neck results more evident. The couple 74–75 and 55–150 always showed the highest and the lowest thermal conductivity, respectively. The thermal conductivity for all couples of particles increases by the time (temperature), according to the neck growth. Averagely, the thermal conductivity of the PB structure was calculated to be 0.86±0.02 $Wm^{-1}K^{-1}$, 1.12±0.06 $Wm^{-1}K^{-1}$, 1.28 ±0.07 $Wm^{-1}K^{-1}$and 1.44±0.08 $Wm^{-1}K^{-1}$at 0.5, 3.5 s, 6.5 s and 9.5 s,

Table 6
Comparison between the thermal conductivity as calculated from the finite element analysis and the proposed model averaged between the values reported in Tables 4 and 5.

t [s]	Temperature at the hot surface [K]	q [W]	λ_{Pow}(FE) [$Wm^{-1}K^{-1}$]	$\lambda_{pow,average}$(analytic) [$Wm^{-1}K^{-1}$] φ =8	$\lambda_{pow,average}$(analytic) [$Wm^{-1}K^{-1}$] φ =4
2.5	964	0.33	4.13	1.29	5.12
5.5	1101	0.42	5.52	1.62	6.10
9.5	1273	0.52	6.50	2.22	7.61

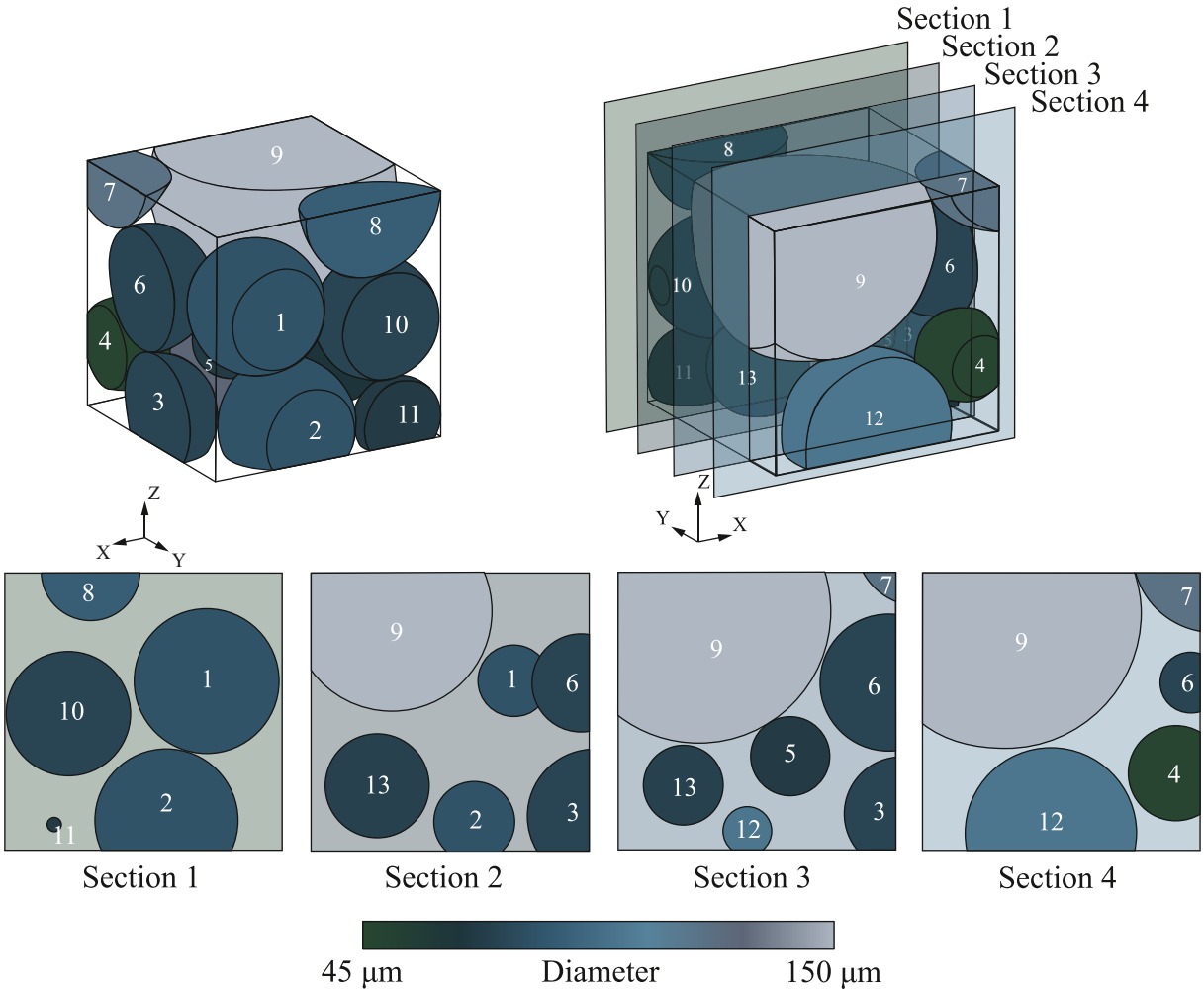

Fig. 11. PB structure and four sections to clarify the spatial distribution of the particles. The colour map of the powder particles indicates different diameters of the powder particles.

respectively.

In the literature, the thermal conductivity of powder beds is usually assumed to be proportional to packing density (relative density) [13,41]. Here, the obtained values of λ_{pow} for the PB structure are lower than BCC, which aligns with this assumption, as BCC has higher packing density compared to PB (n_{BCC}= 0.74 vs n_{PB}=0.66). However, despite the higher density of PB compared to SC, the thermal conductivity of PB is lower than that of SC. For example, with two particles of the same size (80–80) and under the same time calculation (e.g. 9.5 s) so that λ_0 is equal for both structures, PB exhibits thermal conductivity nearly three times lower than SC. This result can be attributed to the fact that PB's thermal conductivity is significantly affected by the presence of pairs of particles with large diameter differences and multiple contact points. These factors, which are captured in the parameter γ, increase the thermal pathways complexity and diminish the impact of the relative density on thermal conductivity.

Therefore, from the perspective of thermal conductivity, a structure composed of particles with uniform diameters, or a narrow size distribution is generally preferred. However, when considering the AM process, a broader particle size distribution is advantageous. A larger variance in particle sizes helps achieve a more uniform material distribution in the powder layer that guarantees the absence of material vacancy during the melting.

Although unambiguous data are lacking, these findings generally align with existing literature on the same material processed by PBF-EB, such as [21,34]. The values in Ref. [21] are slightly lower because the analysis was performed in cold sintered powder, in which the necks could appear smaller because of the shrinkage during the cooling. The values in Ref [34] are generally slightly higher with respect to the results obtained in this work because the neck was considered constant and the

Table 7
Diameters of the powder particles composing the PB structure.

Particle	Diameter [μm]
1	80
2	80
3	75
4	50
5	55
6	75
7	105
8	90
9	150
10	75
11	55
12	100
13	60

Table 8
Neck radius (x) between the couples of powder particles formed by Particle 1 and Particles 2 at 0.5 s, 3.5 s, 6.5 s and 9.5 s.

Couple of particles		Couple ID	0.5 s	3.5 s	6.5 s	9.5 s
Particle 1	Particle 2		x [μm]	x [μm]	x [μm]	x [μm]
1	2	80–80	3.84	6.80	7.95	8.62
1	6	80–75	3.82	9.34	9.12	9.68
1	9	80–150	4.62	10.85	10.48	11.22
2	3	80–74	3.82	9.34	9.12	9.68
2	11	80–52	2.79	8.37	8.30	9.22
3	6	74–75	3.74	9.24	9.00	9.70
3	4	74–49	3.39	8.12	8.33	8.91
4	12	49–100	3.65	7.54	8.71	9.42
4	6	49–75	3.39	7.16	8.34	8.92
5	9	55–150	4.09	9.73	8.70	10.08
5	12	55–100	3.75	7.72	8.89	9.63
6	7	75–105	4.15	10.23	9.70	10.52
6	9	75–150	4.53	11.10	10.35	11.35
7	9	105–150	4.98	12.43	11.71	12.03
8	9	90–150	4.78	11.92	9.69	11.52
8	10	90–73	3.94	9.705	9.49	10.15
9	10	150–73	4.50	10.64	10.33	10.98
9	12	150–100	4.92	12.25	11.09	11.90
9	13	150–60	4.21	9.93	9.91	10.31
10	11	73–52	3.41	8.28	8.26	8.86
10	13	73–60	3.53	8.65	8.65	9.25

arrangement considered for the particles was a BCC structure with particles of equal size. The results of this work are lower than the one reported in Ref [2] as they considered a random arrangement of particles with the same diameter that overlap each other to ensure heat conduction. In comparison with experimental data for PBF-EB (vacuum and growing temperature) reported in Ref. [20], those are slightly higher with respect to the obtained values, because the experiments considered a sample sintered using PBF-EB, which is (re)exposed to high temperatures during the laser flash measurement. This may have caused a further growth of the necks, which justified the slightly higher thermal conductivity.

4. Conclusions

Thermal conductivity in a partially sintered powder bed is a multi-scale phenomenon that occurs at the microscale among powder particles

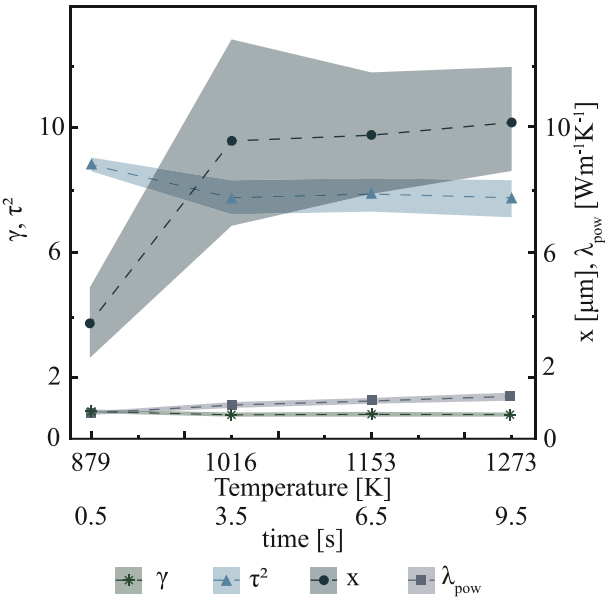

Fig. 12. Interval of variation of x, τ^2 and λ_{pow} considering all the couples of the powder bed. The dashed lines represent the mean value for these quantities at each time step.

Table 9
Values of γ, τ^2 and λ_{pow} where the subscript indicated the time step of the sintering of the PB structure.

Couple ID	$\gamma_{0.5}$	$\tau^2_{0.5}$	$\lambda_{pow0.5}$ [$Wm^{-1}K^{-1}$]	$\gamma_{3.5}$	$\tau^2_{3.5}$	$\lambda_{pow3.5}$ [$Wm^{-1}K^{-1}$]	$\gamma_{6.5}$	$\tau^2_{6.5}$	$\lambda_{pow6.5}$ [$Wm^{-1}K^{-1}$]	$\gamma_{6.5}$	$\tau^2_{9.5}$	$\lambda_{pow9.5}$ [$Wm^{-1}K^{-1}$]
80–80	0.90	8.64	0.88	0.83	7.97	1.10	0.8	7.68	1.30	0.78	7.49	1.47
80–75	0.90	8.64	0.88	0.77	7.39	1.19	0.77	7.39	1.35	0.76	7.30	1.51
80–150	0.94	9.03	0.84	0.86	8.26	1.07	0.86	8.26	1.21	0.85	8.16	1.35
80–74	0.90	8.64	0.88	0.77	7.39	1.19	0.77	7.39	1.35	0.76	7.30	1.51
80–52	0.93	8.93	0.85	0.79	7.59	1.16	0.79	7.59	1.32	0.77	7.39	1.49
74–75	0.90	8.64	0.88	0.75	7.20	1.22	0.76	7.30	1.37	0.74	7.11	1.55
74–49	0.91	8.74	0.87	0.78	7.49	1.17	0.77	7.39	1.35	0.76	7.30	1.51
49–100	0.93	8.93	0.85	0.85	8.16	1.08	0.83	7.97	1.25	0.81	7.78	1.42
49–75	0.91	8.74	0.87	0.81	7.78	1.13	0.78	7.49	1.33	0.76	7.30	1.51
55–150	0.95	9.12	0.83	0.87	8.35	1.05	0.88	8.45	1.18	0.87	8.35	1.32
55–100	0.93	8.93	0.85	0.85	8.16	1.08	0.82	7.87	1.27	0.81	7.78	1.42
75–105	0.92	8.83	0.86	0.81	7.78	1.13	0.82	7.87	1.27	0.8	7.68	1.44
75–150	0.94	9.03	0.84	0.85	8.16	1.08	0.86	8.26	1.21	0.85	8.16	1.35
105–150	0.93	8.93	0.85	0.83	7.97	1.10	0.84	8.07	1.24	0.84	8.07	1.37
90–150	0.94	9.03	0.84	0.84	8.07	1.09	0.87	8.35	1.20	0.85	8.16	1.35
90–73	0.91	8.74	0.87	0.78	7.49	1.17	0.79	7.59	1.32	0.77	7.39	1.49
150–73	0.94	9.03	0.84	0.86	8.26	1.07	0.86	8.26	1.21	0.85	8.16	1.35
150–100	0.93	8.93	0.85	0.84	8.07	1.09	0.85	8.16	1.22	0.84	8.07	1.37
150–60	0.94	9.03	0.84	0.87	8.35	1.05	0.87	8.35	1.20	0.86	8.26	1.34
73–52	0.91	8.74	0.87	0.77	7.39	1.19	0.77	7.39	1.35	0.76	7.30	1.51
73–60	0.90	8.64	0.88	0.76	7.30	1.21	0.76	7.30	1.37	0.75	7.20	1.53

and extends to the whole powder bed. One of the most critical characteristics revealed by past research is that the overall thermal conductivity should be regarded as a structural property rather than an intrinsic thermal property of the material. From an engineering perspective, predicting only the macroscopic properties of multiscale phenomena is often sufficient. In addition, the dependence of the thermal conductivity on the temperature in a power bed cannot be considered without accounting for the neck growth and its effect on the heat flow through the particles.

With this focus, this study proposed a new formulation to evaluate the thermal conductivity of the powder bed using a novel definition of the tortuosity of the heat diffusion path. The model requires only data on the structure geometry, dimension of the neck among the powder particles and its evolution over time. This type of calculation can be applied at each stage of the sintering to obtain the complete characterisation of the thermal conductivity at different sintering degrees of the preheating step of the PBF-EB process. The proposed approach was applied to powder particles arranged in structures with a growing number of powder particles and heat path complexity: an SC, a BCC, and a PB structure. These applications of the model showed the capability of the model to capture the combined effects of several parameters, such as the particle diameters, the neck size, the particle arrangement and the packing density.

The initial stage of the sintering is a bottleneck for the whole process. When the neck is formed and rapidly increases, the thermal conductivity increases. However, the importance of the neck formation increases with the differentiation between the diameter of the particles and the packing density. This can be observed when comparing SC with PB. Despite a lower packing density, the SC structure showed a higher thermal conductivity value compared to the PB structure because SC is composed of powder particles with the same diameter. This result is reasonable if it is considered that the heat flow is facilitated when the neck grows through particles with comparable diameters. The same result is observed in couples with comparable diameters in the PB structure. When the net is constituted by particles with various diameters, the packing density appears to be relevant, which agrees with the previous literature data. In particular, by increasing the packing density, the average contact thermal conductivity of the structure is higher (BCC with $n = 0.72$ vs PB with $n = 0.66$). For all the structures, the growth of the neck size has determined a significant increasing thermal conductivity compared to the loose powder (e.g. 0.2 $Wm^{-1}K^{-1}$) [6].

The results from the proposed model showed an excellent agreement with previous data from the literature. The slight deviations are explained by the environmental or process conditions for the literature data, which are diverse from the PBF-EB, and neck growth was not considered. Therefore, the model could be considered valid.

The verification with the FE model highlighted a strong effect of the parameter φ, suggesting that the assumption of using the maximum coordination number may become limiting when analysing structures with particles with highly differences in terms of contact points. While the proposed simple formulation already provides some insight into thermal conductivity, further reflection is needed to enhance the local information on thermal conductivity.

It also should be noted that the process conditions considered in this work referred to the fast sintering occurring during the short preheating duration. In this case, therefore, the neck growth phenomenon is still far from the plateau region. This stage indicates the closure of the internal pores and requires other cooperative physical processes behind the pure diffusion, such as particle translation as particles fuse [42]. Therefore, the analysis of the powder behaviour under longer sintering needs to consider the relevant pore shrinkage due to the particle translational motion, which also affects the morphological evolution of the particles [42]. Owing to this phenomenon, the relative density (n), considered constant in this work, should be calculated accordingly.

On the other hand, owing to its ease of use, the model's applicability could be extended and verified for other processes based on fast sintering or long sintering conditions at the initial stage.

CRediT authorship contribution statement

Giovanni Rizza: Methodology, Validation, Formal analysis, Data curation, Writing – original draft, Visualization. **Manuela Galati:** Conceptualization, Methodology, Validation, Formal analysis, Resources, Data curation, Writing – review & editing, Supervision.

Declaration of competing interest

The authors declare that they have no known competing financial interests or personal relationships that could have appeared to influence the work reported in this paper.

Data availability

Data will be made available on request.

References

[1] M.R. Alkahari, T. Furumoto, T. Ueda, et al., Thermal conductivity of metal powder and consolidated material fabricated via selective laser melting, Key Eng. Mater. 523–524 (2012) 244–249, https://doi.org/10.4028/www.scientific.net/KEM.523-524.244.
[2] M. Jamshidinia, F. Kong, R. Kovacevic, Numerical modeling of heat distribution in the electron beam melting® of Ti-6Al-4V, J. Manuf. Sci. Eng. 135 (2013), https://doi.org/10.1115/1.4025746.
[3] M. Galati, G. Rizza, S. Defanti, L. Denti, Surface roughness prediction model for Electron Beam Melting (EBM) processing, Ti6Al4V. Precision Eng. 69 (2021) 19–28, https://doi.org/10.1016/j.precisioneng.2021.01.002.
[4] S. Zhang, B. Lane, J. Whiting, K. Chou, An investigation into metallic powder thermal conductivity in laser powder bed fusion additive manufacturing. In: solid Freeform Fabrication 2018, in: Proceedings of the 29th Annual International Solid Freeform Fabrication Symposium - An Additive Manufacturing Conference, SFF 2018, 2020, pp. 1796–1807.
[5] S. Zhang, B. Lane, J. Whiting, K. Chou, On thermal properties of metallic powder in laser powder bed fusion additive manufacturing, J. Manuf. Process. 47 (2019) 382–392, https://doi.org/10.1016/j.jmapro.2019.09.012.
[6] L.C. Wei, L.E. Ehrlich, M.J. Powell-Palm, et al., Thermal conductivity of metal powders for powder bed additive manufacturing, Addit. Manuf. 21 (2018) 201–208, https://doi.org/10.1016/J.ADDMA.2018.02.002.
[7] C. Körner, Additive manufacturing of metallic components by selective electron beam melting — A review, Int. Mater. Rev. 61 (2016) 361–377, https://doi.org/10.1080/09506608.2016.1176289.
[8] P.M. Cordero, J. Mireles, S. Ridwan, R.B. Wicker, Evaluation of monitoring methods for electron beam melting powder bed fusion additive manufacturing technology, Prog Addit Manuf 2 (2017) 1–10, https://doi.org/10.1007/s40964-016-0015-6.
[9] M. Liu, L.N.S. Chiu, H. Shen, et al., Effective thermal conductivities of metal powders for additive manufacturing, Powder. Technol. 401 (2022) 117323, https://doi.org/10.1016/J.POWTEC.2022.117323.
[10] G. Buonanno, A. Carotenuto, G. Giovinco, N. Massarotti, Experimental and theoretical modeling of the effective thermal conductivity of rough steel spheroid packed beds, J. Heat. Transfer. 125 (2003) 693–702, https://doi.org/10.1115/1.1578504.
[11] M. Bahrami, M.M. Yovanovich, J.R. Culham, Effective thermal conductivity of rough spherical packed beds, Int. J. Heat. Mass Transf. 49 (2006) 3691–3701, https://doi.org/10.1016/j.ijheatmasstransfer.2006.02.021.
[12] G.J. Cheng, A.B. Yu, P. Zulli, Evaluation of effective thermal conductivity from the structure of a packed bed, Chem. Eng. Sci. 54 (1999) 4199–4209, https://doi.org/10.1016/S0009-2509(99)00125-6.
[13] E. Tsotsas, H. Martin, Thermal conductivity of packed beds: a review, Chem. Eng. Process. Process Intensification 22 (1987) 19–37, https://doi.org/10.1016/0255-2701(87)80025-9.
[14] N. Hirosaki, Y. Okamoto, M. Ando, et al., Thermal conductivity of gas-pressure-sintered silicon nitride, J. Am Ceram. Soc. 79 (1996) 2878–2882, https://doi.org/10.1111/j.1151-2916.1996.tb08721.x.
[15] S.J. Rodrigues, N. Vorhauer-Huget, E. Tsotsas, Prediction of effective thermal conductivity of packed beds of polyhedral particles, Powder. Technol. 430 (2023) 118997, https://doi.org/10.1016/j.powtec.2023.118997.
[16] M.A. Presley, P.R. Christensen, Thermal conductivity measurements of particulate materials 1. A review, J. Geophys. Research E Planets 102 (1997) 6535–6549, https://doi.org/10.1029/96JE03302.
[17] X. Gong, B. Cheng, S. Price, K. Chou, Powder-bed electron-beam-melting additive manufacturing: powder characterization, process simulation and metrology, in: Early Career Technical Conference, Birmingham, AL, 2013, pp. 55–66.

[18] Neira Arce A (2012) Thermal Modeling and Simulation of Electron Beam Melting for Rapid Prototyping on Ti6Al4V Alloys.
[19] C.J. Smith, S. Tammas-Williams, E. Hernandez-Nava, I. Todd, Tailoring the thermal conductivity of the powder bed in Electron Beam Melting (EBM) Additive Manufacturing, Sci. Rep. 7 (2017) 1–8, https://doi.org/10.1038/s41598-017-11243-8.
[20] M. Galati, E. Campagnoli, V. Giaretto, L. Iuliano, Modelling the thermal behaviour of Ti6Al4V sintered powder bed in electron beam powder bed fusion (EB-PBF), Procedia CIRP. 118 (2023) 664–669, https://doi.org/10.1016/J.PROCIR.2023.06.114.
[21] C.L.A. Leung, R. Tosi, E. Muzangaza, et al., Effect of preheating on the thermal, microstructural and mechanical properties of selective electron beam melted Ti-6Al-4V components, Mater. Des. 174 (2019) 107792, https://doi.org/10.1016/J.MATDES.2019.107792.
[22] A.V. Gusarov, E.P. Kovalev, Model of thermal conductivity in powder beds, Phys. Review B Condens Matter Mater. Phys. 80 (2009) 024202, https://doi.org/10.1103/PHYSREVB.80.024202/FIGURES/14/MEDIUM.
[23] S.J. Cooper, A. Bertei, P.R. Shearing, et al., TauFactor: an open-source application for calculating tortuosity factors from tomographic data, SoftwareX. 5 (2016) 203–210, https://doi.org/10.1016/J.SOFTX.2016.09.002.
[24] B.L. Chua, H.J. Lee, D.G. Ahn, Estimation of effective thermal conductivity of Ti-6Al-4V powders for a powder bed fusion process using finite element analysis, Int. J. Precision Eng. Manuf. 19 (2 19) (2018) 257–264, https://doi.org/10.1007/S12541-018-0030-2, 2018.
[25] A.V. Gusarov, T. Laoui, L. Froyen, V.I. Titov, Contact thermal conductivity of a powder bed in selective laser sintering, Int. J. Heat. Mass Transf. 46 (2003) 1103–1109, https://doi.org/10.1016/S0017-9310(02)00370-8.
[26] J. Grose, M. Cullinan, O.G. Dibua, et al., Simulation and characterization of nanoparticle thermal conductivity for a microscale selective laser sintering system, in: Proceedings of the ASME 2021 16th International Manufacturing Science and Engineering Conference, MSEC 2021, 2021, https://doi.org/10.1115/MSEC2021-64048, 2.
[27] G. Rizza, M. Galati, L. Iuliano, A phase-field study of neck growth in electron beam powder bed fusion (EB-PBF) process of Ti6Al4V powders under different processing conditions, Int. J. Adv. Manuf. Technol. 123 (2022) 855–873, https://doi.org/10.1007/s00170-022-10204-4.
[28] J. Bear, Dinamics of Fluids in Porous Media, American Elesevier Publishing Company, Inc., New York NY, 1972.
[29] M.M. Ahmadi, S. Mohammadi, A.N. Hayati, Analytical derivation of tortuosity and permeability of monosized spheres: a volume averaging approach, Phys. Review E Statis. Nonlinear, Soft Matter Phys. 83 (2011) 1–8, https://doi.org/10.1103/PhysRevE.83.026312.
[30] J.M. Montes, F.G. Cuevas, J. Cintas, Electrical and thermal tortuosity in powder compacts, Granul. Matter. 9 (2007) 401–406, https://doi.org/10.1007/s10035-007-0061-3.
[31] B. Ghanbarian, A.G. Hunt, R.P. Ewing, M. Sahimi, Tortuosity in porous media: a critical review, Soil Sci. Soc. Am. J. 77 (2013) 1461–1477, https://doi.org/10.2136/sssaj2012.0435.
[32] N. Epstein, On tortuosity and the tortuosity factor in flow and diffusion through porous media, Chem. Eng. Sci. 44 (1989) 777–779, https://doi.org/10.1016/0009-2509(89)85053-5.
[33] W.W.M. Siu, S.K. Lee, Effective conductivity computation of a packed bed using constriction resistance and contact angle effects, Int. J. Heat. Mass Transf. 43 (2000) 3917–3924, https://doi.org/10.1016/S0017-9310(00)00051-X.
[34] M. Galati, L. Iuliano, A. Salmi, E. Atzeni, Modelling energy source and powder properties for the development of a thermal FE model of the EBM additive manufacturing process, Addit. Manuf. 14 (2017) 49–59, https://doi.org/10.1016/j.addma.2017.01.001.
[35] M. Galati, A. Snis, L. Iuliano, Experimental validation of a numerical thermal model of the EBM process for Ti6Al4V, Comput. Math. Appl. 78 (2019) 2417–2427, https://doi.org/10.1016/j.camwa.2018.07.020.
[36] H.B. Qi, Y.N. Yan, F. Lin, R.J. Zhang, Scanning method of filling lines in electron beam selective melting, Proc. Inst. Mech. Eng. Part B J. Eng. Manuf. 221 (2007) 1685–1694, https://doi.org/10.1243/09544054JEM913.
[37] G. Rizza, M. Galati, P. Antonioni, L. Iuliano, Effect of the sintering conditions on the neck growth during the powder bed fusion with electron beam (PBF-EB) process, J. Manuf. Mater. Process. 7 (2023) 55, https://doi.org/10.3390/JMMP7020055, 2023Page7:55.
[38] L. Qian, X. Pang, J. Zhou, et al., Theoretical model and finite element simulation on the effective thermal conductivity of particulate composite materials, Compos. Part B Eng. 116 (2017) 291–297, https://doi.org/10.1016/j.compositesb.2016.10.067.
[39] K.Q. Li, D.Q Li, Y. Liu, Meso-scale investigations on the effective thermal conductivity of multi-phase materials using the finite element method, Int. J. Heat. Mass Transf. 151 (2020) 119383, https://doi.org/10.1016/j.ijheatmasstransfer.2020.119383.
[40] M. Koike, K. Martinez, L. Guo, et al., Evaluation of titanium alloy fabricated using electron beam melting system for dental applications, J. Mater. Process. Technol. 211 (2011) 1400–1408, https://doi.org/10.1016/j.jmatprotec.2011.03.013.
[41] C.T. Hsu, P. Cheng, K.W. Wong, Modified Zehner-Schlunder models for stagnant thermal conductivity of porous media, Int. J. Heat. Mass Transf. 37 (1994) 2751–2759, https://doi.org/10.1016/0017-9310(94)90392-1.
[42] R. Shi, M. Wood, T.W. Heo, et al., Towards understanding particle rigid-body motion during solid-state sintering, J. Eur. Ceram. Soc. 41 (2021) 211–231, https://doi.org/10.1016/j.jeurceramsoc.2021.09.039.